JOURNAL OF MATERIALS SCIENCE 28 (1993) 3482–3488

Influence of the calcining temperature on the sintering and properties of PZT ceramics

M. VILLEGAS, C. MOURE, J. R. JURADO, P. DURÁN
Instituto de Cerámica y Vidrio, CSIC, Electroceramics Department, Madrid, Spain

Niobia-doped PZT powders were prepared by both hydroxide and oxalate coprecipitation methods. The resulting amorphous powders were calcined at two different temperatures (550 and 700 °C) and the morphology and size of the calcined particles were studied. It was found that hydroxide powders, when calcined at 700 °C, gave 98% theoretical density, d_{th}, bodies at a sintering temperature as low as 1100 °C in air. The high agglomeration present in oxalate powders strongly retarded densification. Of the piezoelectric properties, a k_p higher than 60% and a d_{33} constant of 360×10^{-12} CN^{-1} were measured. Dielectric parameters T_c and k_{3T}, 310 ° C and 1100, respectively, were determined.

1. Introduction

One of the most important problems in fabricating reliable PZT ceramics is the volatility of PbO. The loss of PbO during both the calcination and sintering steps leads to fluctuation in the PZT composition which, in turn, will strongly affect the sintering process itself and the electromechanical properties. In such a way, two methods to control the PbO activity are commonly used: (a) by adding a PbO excess to the PZT composition and embedding the sample in an adequate buffer, and (b) by sintering the PZT samples at a temperature sufficiently low for the PbO activity to be negligible. In the first method, it is generally assumed that an excess of PbO is necessary for achieving highly densified PZT ceramics [1–3]; nevertheless, the use of an adequate atmosphere powder, as well as a sufficient amount of buffer to equilibrate the PbO-vapour phase through the sintering process, are also required. Although widely studied in the 1970s [4–6], even today this question remains permanently open to discussion. For example, Kingon and Clark [7] reported results in which a PbO-deficient PZT showed a higher densification than that containing an excess of PbO.

The second method uses a non-conventional preparation process in which the characteristics of the initial powder will allow the production of almost theoretically dense bodies at a sintering temperature as low as possible. In this sense, significant progress has been made using different wet-chemical methods for preparing submicrometre-sized ferroelectric powders [8, 9], in which controlled stoichiometry, impurity content, and microstructure of the sintered bodies could be achieved.

However, no systematic work to relate the processing parameters to behaviour properties has yet been reported; therefore the present work was undertaken to study the effect of calcination temperature on the morphology of the calcined powders, compaction behaviour, sintering and piezoelectric properties of niobia-doped PZT prepared by a wet-chemical method.

2. Experimental procedure

Fig. 1 shows the flow diagram of the two methods employed to synthesize the PZT powders with composition Pb $(Zr_{0.53}Ti_{0.455}Nb_{0.015})O_3$ + 3 wt % PbO from the raw-material selection up to the sintering stage. The powders obtained were labelled CH for hydroxide powder and CO for the oxalate one.

The raw materials were commercial reagents of high purity. The synthesis was performed by calcining the coprecipitated powders at two different temperatures: 550 °C/56 h (LTC) and 700 °C/2 h (HTC) for both preparation techniques. These temperatures were chosen by taking into account that at 550 and 700 °C the resulting PZT powders were totally formed, as can be seen from the X-ray diffraction and differential thermal analysis–thermogravimetry (DTA–TG) studies (Fig. 2), and therefore the subsequent behaviour of the powders, with different particle size and specific surface area, could be compared.

The coprecipitated and calcined powders were analysed by X-ray diffraction, transmission electron microscopy (TEM), scanning electron microscopy (SEM) and sedigraph.

After calcining, the powders were milled, sieved and isopressed to discs of about 2 cm diameter and 0.5 cm thick. Fig. 3 shows the crucible used for sintering in the PbO atmosphere. The buffer employed was PZT + 1%PbO.

On sintered samples, the apparent density was measured using Archimedes' method. The phases present after sintering were identified by XRD and their lattice parameters were determined using silicon as internal standard. Microstructure was studied by SEM on both polished and chemically etched and

0022–2461

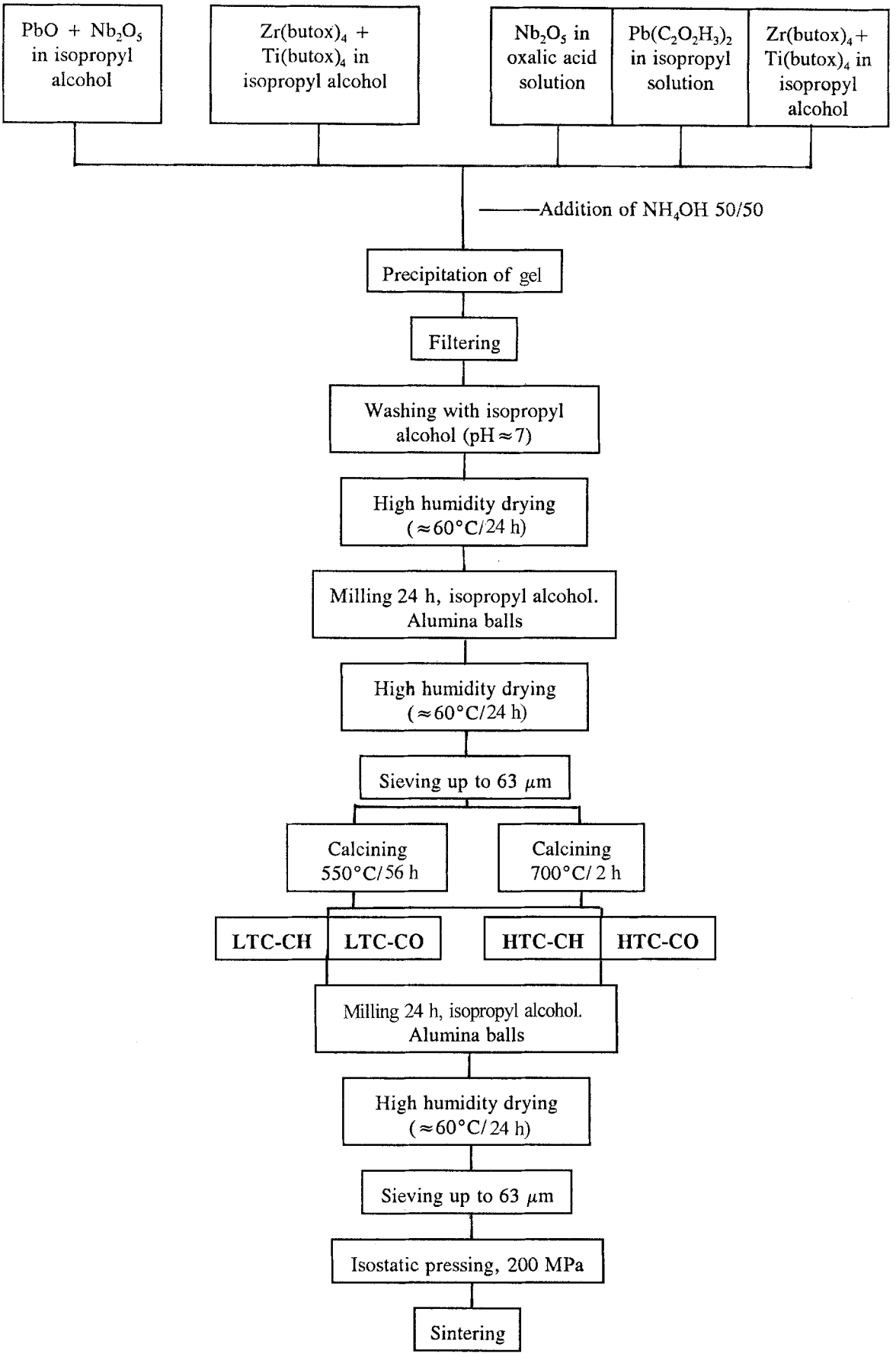

Figure 1 Flow diagram of the hydroxide and oxalate co-precipitation methods.

freshly fractured surfaces. The grain size was measured from the micrographs by the line interception method. To determine the piezoelectric properties, a selected set of discs was poled at 40 kV cm^{-1} for 0.5 h in a silicone oil bath at 120 °C. The piezoelectric properties were determined by IEEE standards using measurements made with a vectorial impedance analyser HP 4192 A; all calculations were made following the resonance method [10]. To measure d_{33}, a Berlincourt Piezo-d meter was employed.

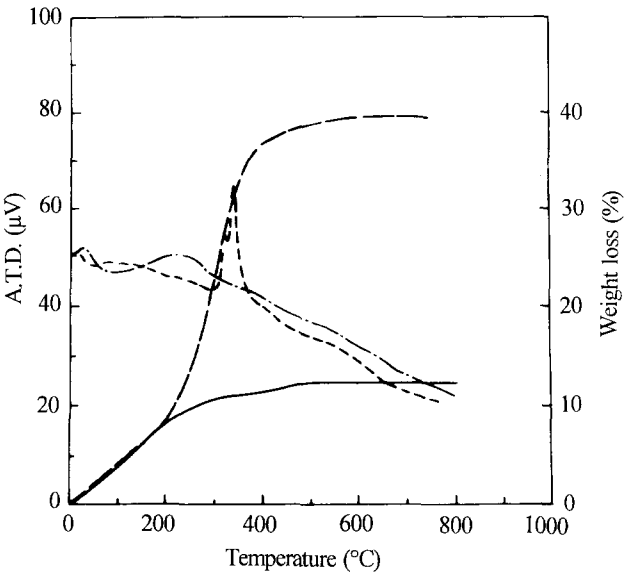

Figure 2 DTA–TG studies of the coprecipitated powders. (——) PZTN–CH, (– – –) PZTN–CO.

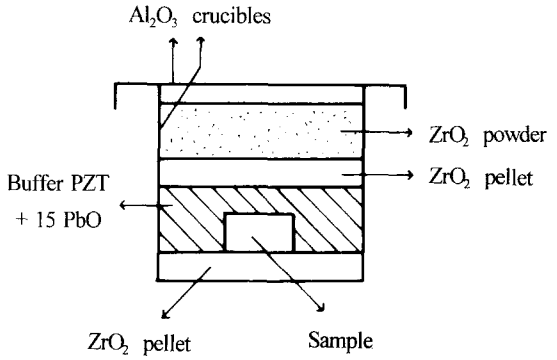

Figure 3 Crucible used in the sintering process.

3. Results and discussion

3.1. Powder synthesis

XRD of the hydroxide-coprecipitated powder showed an amorphous structure, whereas the oxalate powder contained crystalline oxalates. XRD patterns of both calcined powders at high and low temperature presented peaks which corresponded to a perovskite-type phase with rhombohedral symmetry, and a PbO single phase due to the excess PbO added during powder preparation. The lattice parameter of the rhombohedral phase was $a = 0.4080 \pm 0.0005$ nm in all cases. The XRD study also demonstrated that the formation of PZT was complete at both temperatures. Although the composition was formulated in the morphotropic phase boundary, where some authors [11–13] report the coexistence of the tetragonal and rhombohedral phases, the Nb^{5+} addition moves Ti^{4+} from its initial lattice position, thus producing a shift towards the rhombohedral phase.

Coprecipitated and calcined powders were dispersed in ethyl alcohol for observation by transmission electron microscopy. In the coprecipitated powders, gel formation made the observation of primary particle morphology difficult. However, typical TEM pictures of the two LTC powders were obtained. Fig. 4a shows that the LTC–CH powder was composed of large agglomerates of about 1 μm in size. Nevertheless, the primary particle size could be estimated to be around 50 nm. The LTC–CO powder contained island-like agglomerates of less than 0.5 μm but the primary particle size was around 100 nm, as can be seen in Fig. 4b.

The average particle size of the HTC powders was measured by both TEM and SEM techniques. The powder morphology showed a high agglomeration and, in some cases, a premature onset of sintering. There was no particle size difference between TEM and SEM observations but a higher particle agglomeration was present in HTC–CO powders. Average particle sizes of 0.2 and 0.15 μm were measured for HTC–CH and HTC–CO powders, respectively. Fig. 5a and b show scanning electron micrographs of these two powders.

The particle-size distribution curves obtained by using the sedigraph technique (Fig. 6) showed particle sizes at least ten times higher than those obtained from TEM and SEM observations. This could indicate that sizes measured by the sedimentation method are not the primary particle size, but the agglomerate size.

Particle sizes measured by the X-ray line-broadening method did not differ substantially from those obtained by TEM and SEM observations. Specific surface areas were measured by the BET method, and were also calculated by taking into account the particle size and density measured by X-ray analysis. The

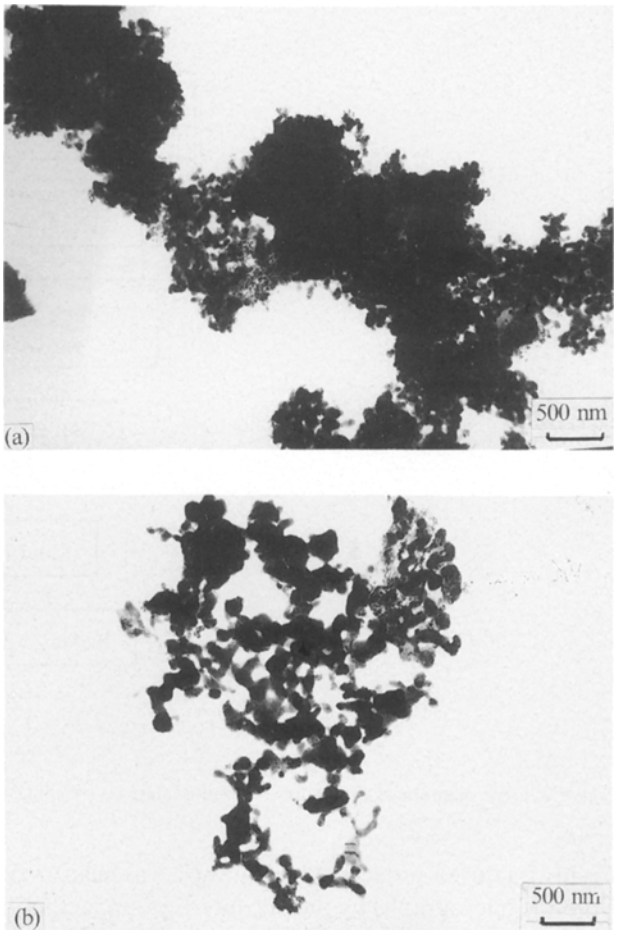

Figure 4 Transmission electron micrographs of (a) LTC–CH and (b) LTC–CO powders.

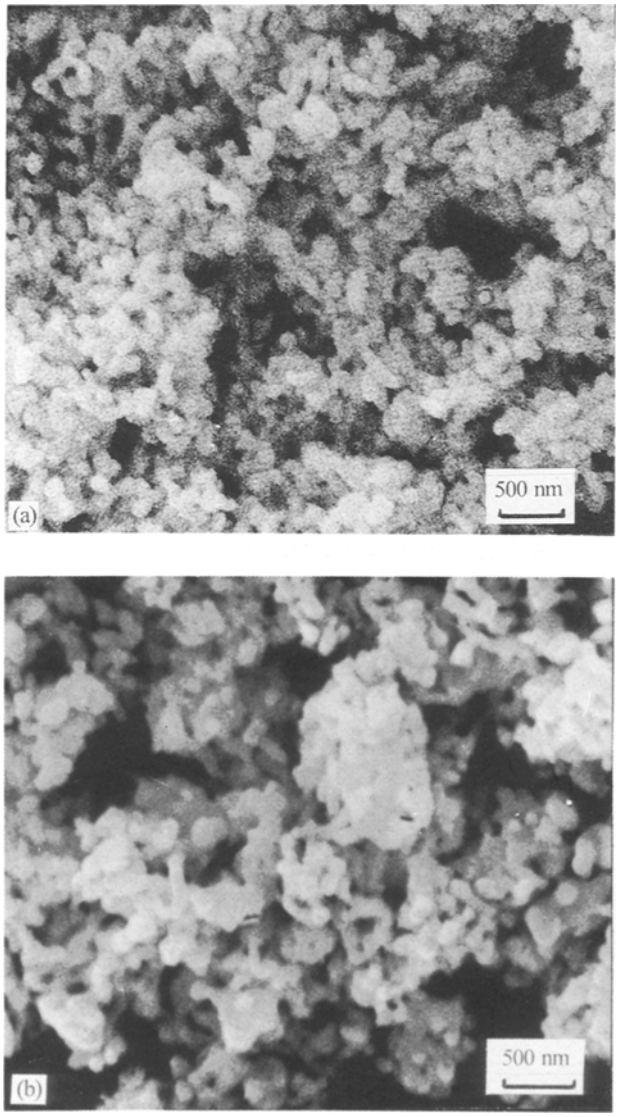

Figure 5 Scanning electron micrographs of (a) HTC–CH and (b) HTC–CO powders.

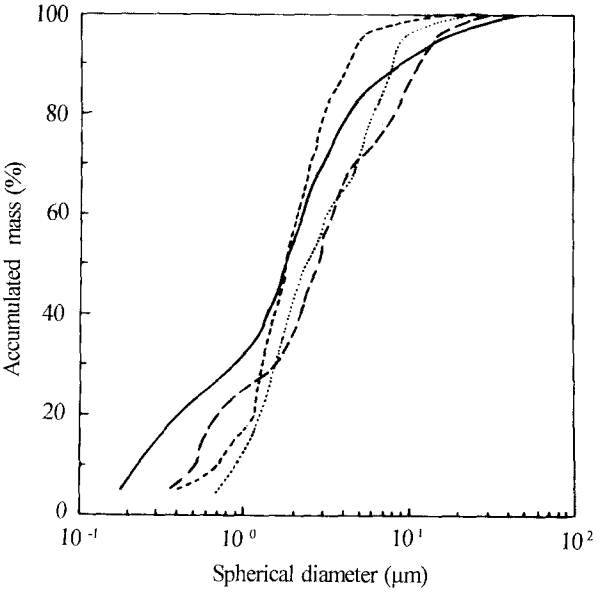

Figure 6 Sedigraph curves for the calcined powders. (——) LTC–CH, (– – –) HTC–CH, (- - -) LTC–CO, (···) HTC–CO.

TABLE I Characteristics of the calcined powders

Samples	Particle size (μm)			Surface area ($m^2\ g^{-1}$)	
	TEM	SEM	XRD	XRD	BET
LTC–CH	0.05	0.07	0.10	75	18
LTC–CO	0.10	0.09	0.12	49	–
HTC–CH	0.16	0.20	0.19	40	8
HTC–CO	0.12	0.15	0.20	38	–

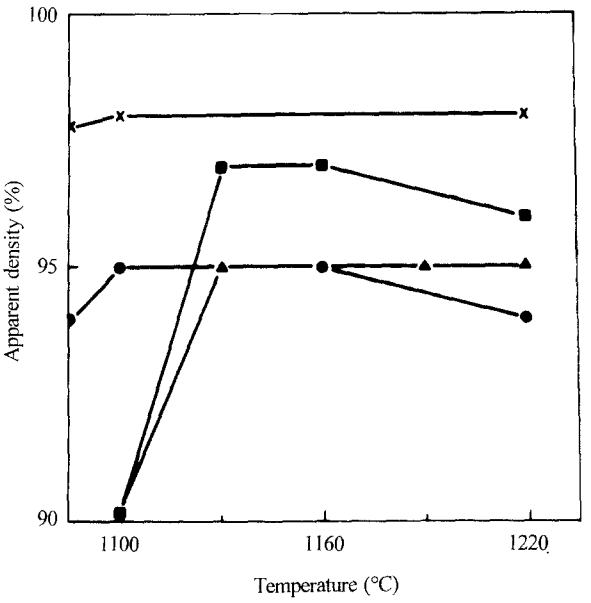

Figure 7 Densification curves of the four calcined powders soaked for 4 h: (X) HTC–CH, (●) LTC–CH, (▲) HTC–CO, (■) LTC–CO.

difference between these two values is caused by the XRD method which considers spherical and totally dispersed particles. Table I compares the different powder parameters as measured by several techniques.

3.2. Sintering

The study of densification and weight loss was carried out as a function of sintering temperature. The temperature range chosen was 1100–1220 °C for 4 h. Fig. 7 shows the densification process of the four kinds of calcined powders; it can be seen that HTC–CH samples were highly densified, $\geqslant 98\%$ theoretical density, d_{th}, at a temperature as low as 1100 °C, and remaining constant through a broad temperature range. LTC–CH samples were less dense $\approx 95\%\ d_{th}$ at 1100 °C. The densification behaviour of both CH samples is similar, reaching a maximum density at low temperature and remaining constant when temperature increases. On the other hand, the LTC–CO sample was also highly dense ($\approx 97\%\ d_{th}$), although this density was reached at a somewhat higher temperature (1130 °C) than that of CH samples. The HTC–CO sample exhibits the same sintering behaviour as the LTC–CO sample with temperature, with $\approx 95\%\ d_{th}$ at 1130 °C.

In the CH powders, although the sinterability of the LTC–CH powder, due to its high specific surface area,

is higher than that of the HTC–CH powder, its densification is lower. However, an exaggerated weight loss was observed during the sintering process, which could produce an increase in the viscosity of the liquid phase owing to its lower PbO concentration causing a decrease in the diffusion rate and thus retarding densification. In the HTC–CH samples, a normal sintering process took place, a small weight gain was present in all cases, and thus the liquid phase viscosity was lower than in the case of the LTC–CH sample, leading to increasing density.

In the CO powders, the higher densification of the LTC–CO samples runs parallel to a powder sinterability higher than that of the HTC–CO powder, although a higher sintering temperature was necessary to achieve a densification level similar to that of HTC–CH sintered samples. In all cases, a weight gain took place during the sintering process.

Table II shows the main physical characteristics of the best CH and CO sintered samples.

TABLE II Physical properties of the sintered samples

Samples	Density (g cm^{-3})	% Weight variation	Grain size (nm)
LTC–CH	7.60	− 3.10	2.5
HTC–CH	7.80	+ 0.03	7.5
LTC–CO	7.75	+ 1.20	3.5
HTC–CO	7.60	+ 0.43	6.0

d_{th} = 8.00 g cm^{-3}.

3.3. Microstructure

Scanning electron micrographs of polished and chemically etched surfaces of LTC–CH sample listed in Table II are shown in Fig. 8a; it can be seen that the microstructure is homogeneous, the average grain size of about 2.5 μm is very uniform, and that the final grain size is well controlled, because the powder particle size is of a nanometre scale and therefore highly

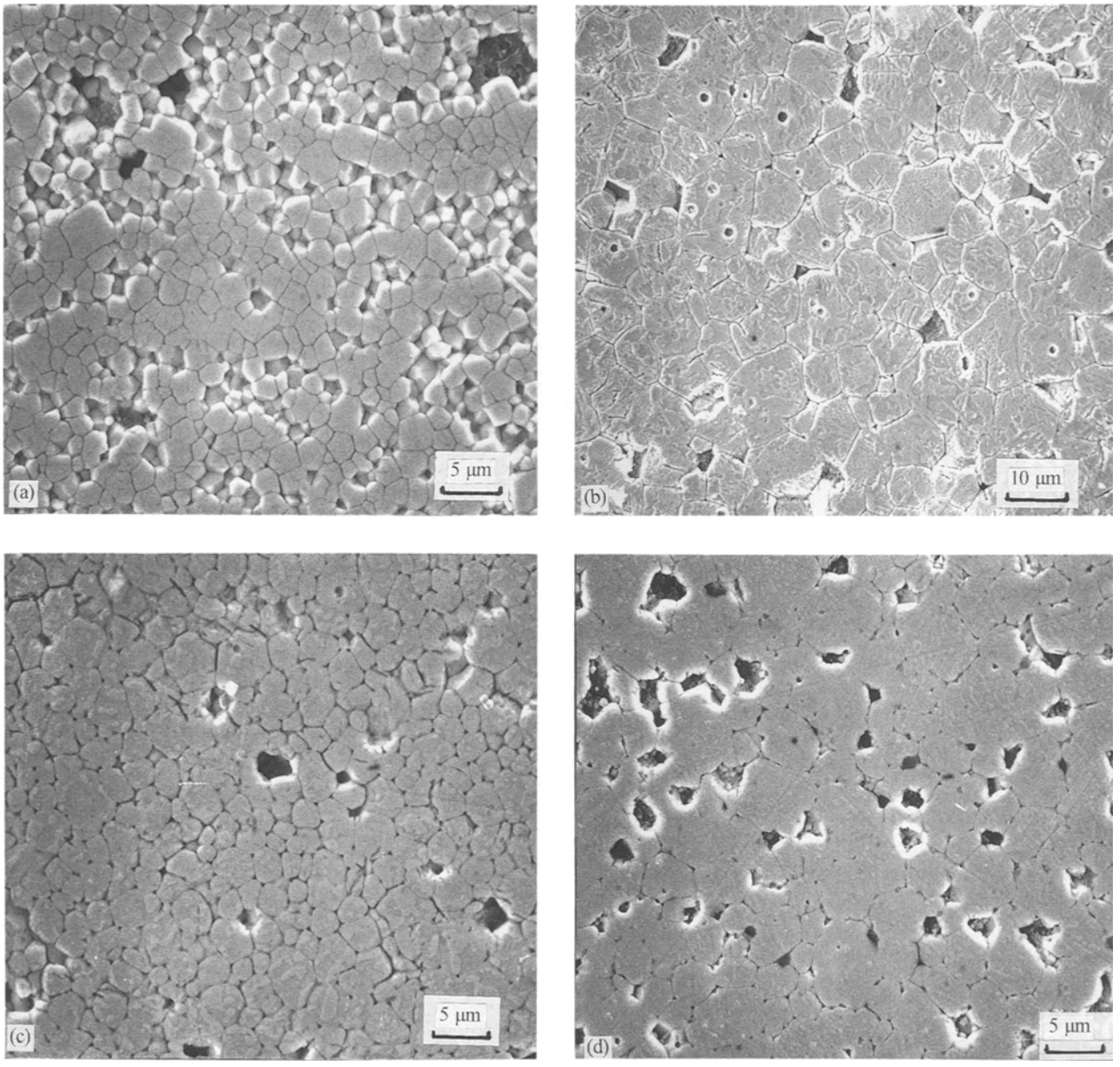

Figure 8 Polished and chemically etched surfaces of compacts sintered at 1160 °C: (a) LTC–CH, (b) HTC–CH, (c) LTC–CO and (d) HTC–CO.

reactive. The micrograph of the LTC–CO sample is shown in Fig. 8b and, in this case, the microstructure is rather homogeneous. The average grain size is slightly higher than that of LTC–CH sample, which could be related to the larger particle size of the calcined oxalate powder.

When the calcining temperature was raised to 700 °C, the microstructure changed significantly, as observed in Fig. 8c (HTC–CH) and d (HTC–CO). The average grain size is quite large, around 7.5 and 6.0 μm, respectively. The microstructure is very homogeneous and in the case of the best densified sample (HTC–CH), there is no significant porosity (97% theoretical density).

On the other hand, the grain shape of HTC samples exhibit well-faceted grains, whereas the LTC grains have a more rounded and smooth morphology, indicating that although LTC microstructures are good, the final grain formation is more complete for HTC microstructures, as is clearly expected from the higher calcining temperature.

In addition, the LTC–CH sample, which is a lead-deficient material, showed a liquid phase which wets both grain boundaries and triple points (Fig. 9a), whereas in the lead-excess materials (Fig. 9b–d) liquid phase goes mainly towards triple points. Therefore, the liquid-phase modified the grain-boundary interfacial energy and, consequently, the dihedral angles. If we consider that the LTC–CH sample had interstitial PbO, which tended to volatilize during sintering (weight loss), the solid–solid and solid–liquid surfacial energy (γ_{SS} and γ_{SL}) is modified by the PbO loss, producing an increase of the γ_{SS}/γ_{SL} ratio with respect to the same relation in the lead-excess samples

$$(\gamma_{SS}/\gamma_{SL})_d > (\gamma_{SS}/\gamma_{SL})_e \quad (1)$$

where d indicates lead-deficient, and e lead-excess material. This change in surfacial energy produced a different wetting in both types of sample

$$(\text{wetting})_d > (\text{wetting})_e \quad (2)$$

The fracture energy is proportional to $\gamma(G = 2\gamma)$, so

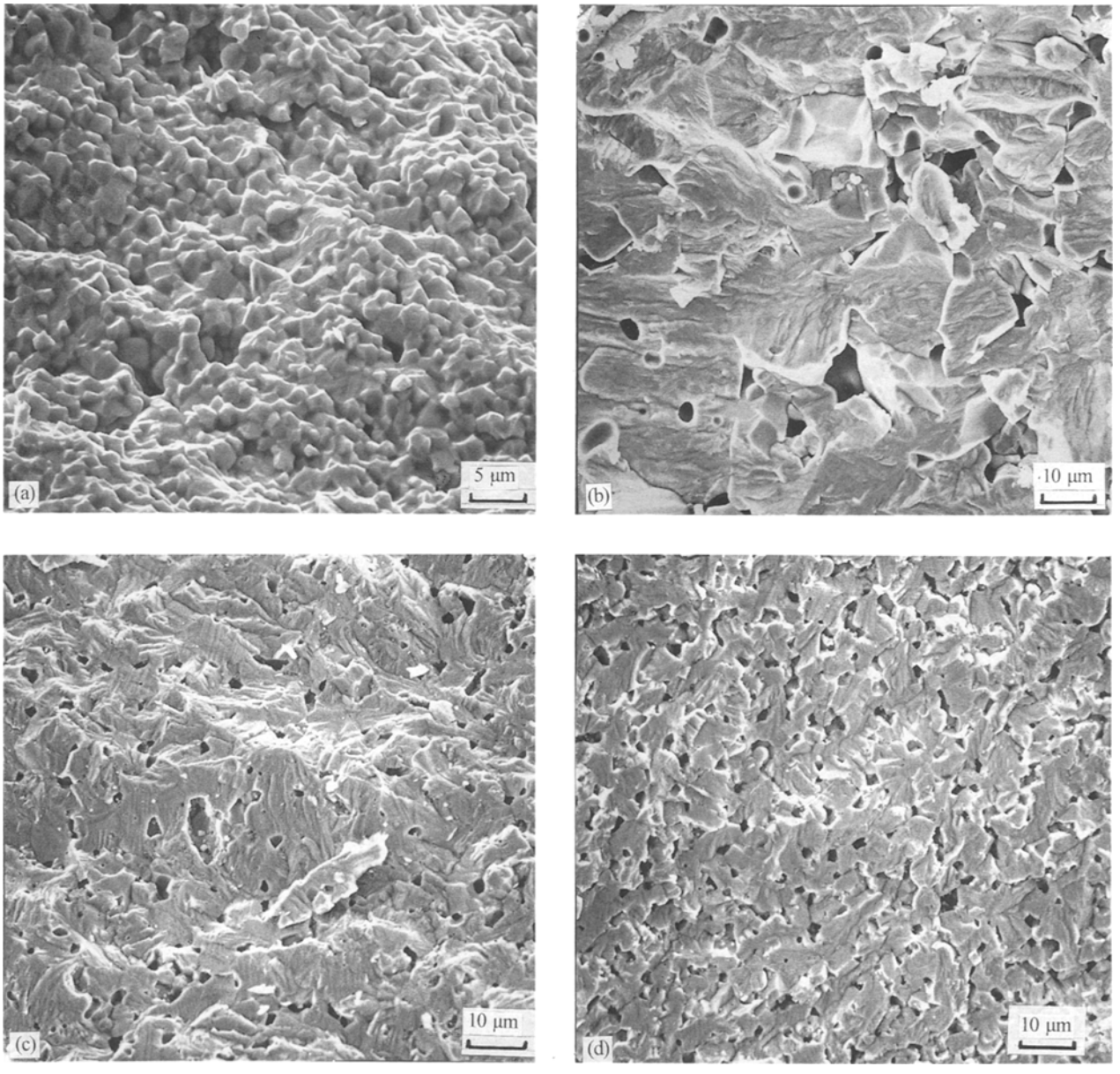

Figure 9 Fracture surfaces of compacts sintered at 1160 °C: (a) LTC–CH, (b) HTC–CH, (c) LTC–CO and (d) HTC–CO.

$G_{SS} > G_{SL}$ in the lead-deficient sample and fracture is intergranular (Fig. 9a), whereas $G_{SS} < G_{SL}$ in lead-excess materials where a transgranular fracture is produced (Fig. 9b–d).

3.4. Dielectric properties

The substitution and interstitial occupation of doping ions are responsible for the piezoelectric properties of these types of sample. If a lead zirconate–titanate composition near the morphotropic phase boundary, $Pb(Zr_{0.53}Ti_{0.47})\ O_3$, is doped with ions which act as donors, A-site vacancies are induced in the ABO_3 perovskite structure [14], and an increase of domain-wall mobility is produced. This, in turn, produces a higher dipole moment for low applied poling field, which leads to better dielectric and piezoelectric properties.

In fact, we have found that in our samples, vacancies in the A-site are produced. In addition to this, when additional lead vacancies are generated, due to PbO loss, an increase of piezoelectric properties (Table III) is produced; this result agrees very well with the suggestions made by Atkin and Fulrath [15].

4. Conclusions

The calcining temperature of PZT powders can be lowered by at least 150 °C when using wet chemical methods to prepare these powders. When the two co-precipitation techniques (hydroxide and oxalate) are compared, we can conclude that the hydroxide method is somewhat better than the oxalate method, although both can be used to obtain PZT powders with high sinterability. The very highly reactive hydroxide powders calcined at 550 °C induce a strong lead deficiency during the densification step, which is simultaneously favoured due to PbO losses. The PbO-deficient material exhibits higher piezoelectric properties (high k_p, ε and d_{33}) and low tan δ. We thus conclude that the control of powder calcination process can play a crucial role in producing PbO-deficient material which, on the other hand, leads to an improvement of electromechanical factors and piezoelectric properties.

TABLE III Electromechanical properties of the four types of materials prepared

Sample	T^a	k_p	K_{3T}	Tan δ	Q_m	k_t	d_{33}
LTC–CH	1190/4	0.61	1303	1.8	76	0.42	360
LTC–CO	1190/4	0.48	595	2.4	73	0.45	153
HTC–CH	1190/4	0.50	629	2.6	84	0.52	196
HTC–CO	1190/4	0.49	544	2.2	92	0.45	190

References

1. F. F. MURRAY and R. H. DUNGAN, *Ceram. Ind.* **82** (1964) 74.
2. G. S. SNOW, *J. Amer. Ceram. Soc.* **56** (1973) 479.
3. *Idem, ibid.* **57** (1974) 272.
4. A. H. WEBSTER, T. B. WESTON and N. F. H. BRIHGT, *ibid.* **50** (1967) 1190.
5. A. D. JAMES and P. F. MESSER, *Trans. J. Brit. Ceram. Soc.* **77** (1978) 152.
6. G. S. SNOW, *J. Amer. Ceram. Soc.* **56** (1972) 91.
7. A. I. KINGON and J. B. CLARK, *ibid.* **66** (1983) 256.
8. L. M. BROWN and K. S. MAZDIYASNI, *ibid.* **55** (1972) 541.
9. H. YAMAMURA, M. TANADA, H. HANEDA, S. SHIRASAKI and Y. MORIYOSHI, *Ceram. Int.* **11** (1985) 23.
10. *Proc. IRE* **49** (1961) 1162.
11. A. BARBULESCU, D. BARB and E. BARBULESCU, *Ferroelectrics* **47** (1986) 221.
12. K. KAKEGAWA and J. MOHRI, *J. Amer. Ceram. Soc.* **65** (1982) 515.
13. S. A. MABUD, *Appl. Crystallogr.* **13** (1980) 211.
14. R. G. GERSON, *J. Appl. Phys.* **31** (1960) 188.
15. R. B. ATKIN and R. M. FULRATH, *J. Amer. Cream. Soc,* **54** (1971) 265.

Received 28 January
and accepted 20 November 1992